

Surface Van Hove Singularity Enabled Efficient Catalysis: The Cases of CO Oxidation and Hydrogen Evolution Reactions

Liangliang Liu^{1,3}, Chunyan Wang^{1,2}, Liying Zhang¹, Chengyan Liu¹, Chunyao Niu²,
Zaiping Zeng¹, Dongwei Ma^{1,3*}, and Yu Jia^{1,2,3*}

¹ Key Laboratory for Special Functional Materials of Ministry of Education, Collaborative Innovation Center of Nano Functional Materials and Applications, School of Materials Science and Engineering, Henan University, Kaifeng 475004, China

² International Laboratory for Quantum Functional Materials of Henan, and School of Physics and Microelectronics, Zhengzhou University, Zhengzhou 450001, China

³ Key Laboratory for Quantum Materials of Henan, and Center for Topological Functional Materials, Henan University, Kaifeng 475004, China

Corresponding Author:

madw@henu.edu.cn (Dongwei Ma), jiayu@henu.edu.cn (Yu Jia)

Abstract: Surface Van Hove singularity (SVHS), defined as the surface states near the Fermi level (E_F) in low-dimensional systems, triggers exciting physical phenomena distinct from bulk. We herein explore theoretically the potential role of SVHS in catalysis taking CO oxidation reaction as prototype over graphene/Ca₂N (Gra/Ca₂N) heterojunction and Pt₂HgSe₃ (001) surface. It is demonstrated that both systems with SVHS could serve as an electron bath to promote O₂ adsorption and subsequent CO oxidation with low energy barriers of 0.2 ~ 0.6 eV for Gra/Ca₂N and Pt₂HgSe₃ (001) surface. Importantly, the catalytically active sites associated with SVHS are well-defined and uniformly distributed over the whole surface plane, which is superior to the commonly adopted defect or doping strategy, and further the chemical reactivity of SVHS also can be tuned easily via adjusting its position with respect to E_F . Our study demonstrates the enabling power of SVHS, and provides novel physical insights into the promising potential role of VHS in designing high-efficiency catalysts.

Key Words: *Surface Van Hove singularity; Catalysis; Localized electronic state; CO*

oxidation; Density functional theory

Van Hove singularity (VHS) is a saddle point in the electronic band structure where the density of states (DOS) diverges logarithmically, exhibiting the most characteristic feature of existing highly localized electronic states¹⁻³. The electronic instability in the vicinity of VHS promotes diverse novel phases of matter, such as superconductivity⁴⁻⁵, ferromagnetism⁶ and charge density wave⁷, which makes the study of VHS physics the research frontier of condensed matter physics and materials science. If the VHS exists in reduced dimensional systems, such as surface systems or two-dimensional (2D) materials, and serve as the surface states near the Fermi level (E_F), we name it as surface Van Hove singularity (SVHS). In stark contrast to the VHS in bulk which is remote from the Fermi level (E_F) and insensitive to external perturbations, SVHS can be tuned to be around or even well-aligned with E_F , delivering rich surface physical and chemical properties waiting for exploration. This can be achieved in a much easier way via surface engineering, such as chemical doping⁸⁻⁹, intercalation¹⁰⁻¹¹, constructing heterojunction¹²⁻¹³, gating¹⁴ or twisting¹⁵⁻¹⁶, thanks to the emergence of novel surface or 2D layered materials with rich characteristics and functionalities.

Various surface or 2D material systems with SVHS have been realized, and intriguing surface or interface phenomena has been subsequently reported, including interface superconductivity, surface charge density wave, and optical adsorption¹⁷⁻²³. Monolayer graphene on SiC substrate or bilayer boron nitride via alkali-metal intercalation enables the appearance of SVHS, which induces the phonon-mediated superconductivity through the strong electron-phonon coupling at the vicinity of SVHS¹⁷⁻¹⁸. Optical absorption has also been found to be significantly enhanced in twisted bilayer graphene with SVHS locating at the E_F , and G band resonance has been

observed¹⁹⁻²¹. Due to the charge transfer from Ca₂N electride, the E_F is pushed up to be well-aligned with the π^* -band VHS of graphene, and hence SVHS with large DOS appears in the graphene/Ca₂N electride (Gra/Ca₂N) heterojunction, as theoretically predicted²⁴. The efficient charge transfer nature has been confirmed by later experiment on heterojunctions formed with multilayered graphene on Ca₂N²⁵. Besides the aforementioned tuning strategies, the recently discovered topological materials with intrinsic surface states close to E_F could natively serve as SVHS, which originates from the nontrivial topological nodal line of the bulk, protected with certain symmetry. A prototypical example is Pt₂HgSe₃ film with cleaved (001) surface²⁶⁻²⁷.

One the peculiar characteristics of the SVHS is the highly localized electronic states²⁻³ that could benefit the charge exchange between them, and thus holds promising potential for efficient catalysis²⁸⁻²⁹. In this contribution, we examine the SVHS catalysis choosing prototypical chemical reactions on ground of the aforementioned two well-established platforms of Gra/Ca₂N heterojunction²⁴ and Pt₂HgSe₃ film with (001) surface²⁶⁻²⁷. All first-principles calculations are performed within the framework of density functional theory using the Vienna *ab initio* simulation package with the projector-augmented wave method³⁰⁻³² (see Computational details in Supporting Information). The reaction barrier is computed using the climbing image nudged elastic band method³³. We demonstrate the enabling power of SVHS on CO oxidation and hydrogen evolution reactions. The SVHS in both systems is found to serve as electron bath to promote O₂ adsorption and subsequent CO oxidation with low kinetic energy barriers of 0.37 eV for Gra/Ca₂N and 0.59 eV for Pt₂HgSe₃. Two features of SVHS catalysis have been further identified. One is that the active sites originating from the SVHS are well-defined and uniformly distributed over the whole surface plane. The other is the tunability of the chemical activity driven by SVHS through adjusting its

relative energy position with respect to E_F as for Gra/ Ca_2N heterojunction. Our study drives Van Hove singularity to the catalytic applications, and provides promising degree of freedom towards the search and design of catalysts.

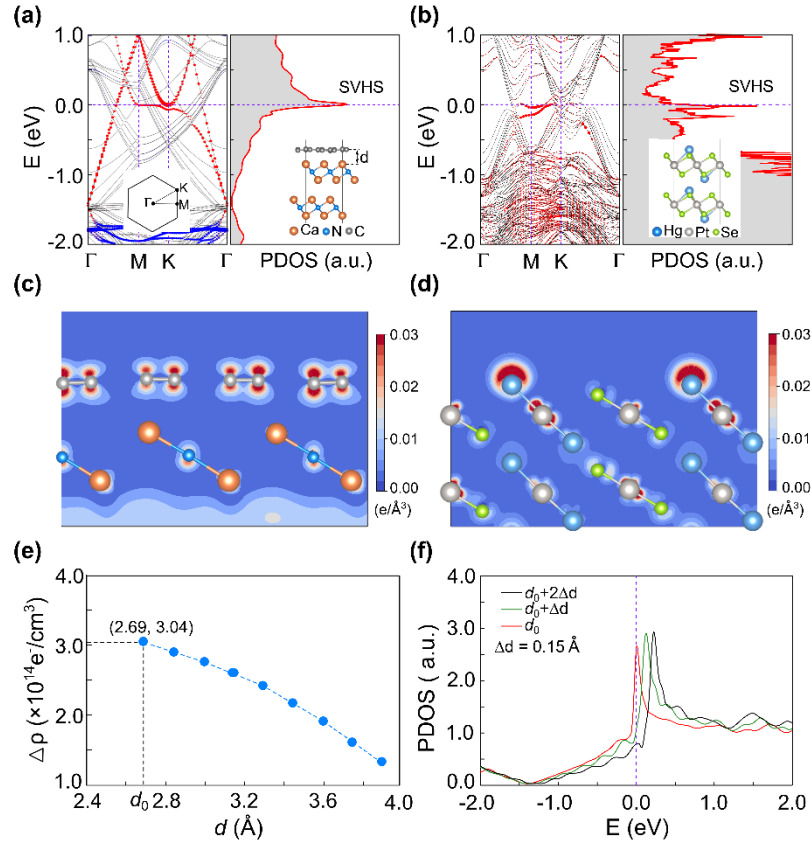


Figure 1: (a) Calculated band structure of the Gra/ Ca_2N and partial DOS (PDOS) for graphene. Here, the bands projected onto graphene and the first Ca_2N atomic layer are respectively displayed with red and blue circles. d is the interlayer distance between graphene and the topmost Ca layer. (b) Surface band structure of a ten-layer thick Pt_2HgSe_3 slab. The bands projected onto the first layer are displayed with red circles. The energy zero represents E_F . (c) and (d) Calculated partial charge density around the SVHS (electron energy between -0.2 and 0 eV) for Gra/ Ca_2N and Pt_2HgSe_3 surfaces respectively, plotted on the (110) face. (e) Net average charge ($\Delta\rho$) and (f) PDOS for the graphene layer in Gra/ Ca_2N heterojunction as a function of the interlayer distance d . In (e) and (f), d_0 is the optimal distance, 2.69 Å.

To begin with, we study the CO oxidation reaction on Gra/Ca₂N heterojunction and Pt₂HgSe₃ (001) surface. The electronic band structures of the proposed systems are given in Figs. 1(a) and (b). In both systems, the SVHS at M-point appears well-aligned with E_F . For Gra/Ca₂N heterojunction, VHS in the free-standing graphene is about 1.6 eV above the E_F ³⁴. Thanks to the strong charge transfer nature of electride, E_F is pushed up, and aligns with the SVHS. As demonstrated by the PDOS, SVHS exhibits a unique feature of large DOS. The charge density plot of Fig. 1(c) shows that the charges for the SVHS are highly localized, distributing mainly on two lobes of the $2p_z$ orbitals of the carbon atoms. For Pt₂HgSe₃ (001) surface, the surface states are nontrivial with a unique saddle-like energy dispersion, and the associated SVHS is natively positioned near the E_F ²⁶⁻²⁷. The presence of SVHS in such a system is also justified by the large DOS near the saddle point [see Fig. 1(b)]. The charges of the SVHS are found to be highly localized on the surface Hg atoms [see Fig. 1(d)]. We further show in Fig. 1(e) the modulation of net charges in graphene as a function of the interlayer spacing d of the Gra/Ca₂N heterojunction. Due to the electron donating from the electride layer, graphene component receives a high n -doping at the optimal distance d_0 , with charge density reaching up to $3.04 \times 10^{14} \text{ e}^-/\text{cm}^2$. Strikingly, the net charge $\Delta\rho$ decreases sublinearly with respect to the interlayer distance d [see Fig. 1(e)]. We note that considerably large net charge density ($> 1 \times 10^{14} \text{ e}^-/\text{cm}^2$) in the graphene layer can be easily reached as long as the interlayer distance is larger than 4 Å. Accordingly, the position of E_F is tuned around the SVHS [see Fig. 1(f)], through which it is expected the chemical and catalytic activity of the graphene layer can be modulated.

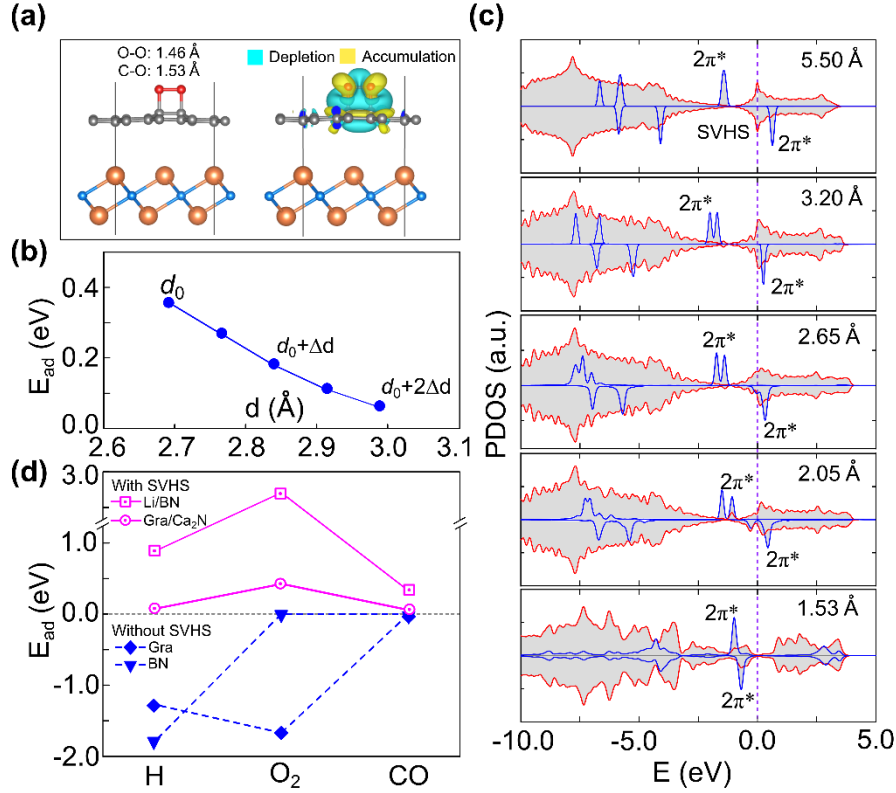


Figure 2: (a) The adsorption configuration and isosurface ($0.015 \text{ e}^-/\text{\AA}^3$) of charge density difference for an O₂ molecule on the Gra/Ca₂N surface. (b) The change of O₂ adsorption energy as a function of interlayer distance d . (c) The PDOS of O₂ (blue line) and graphene (red line) during the process of O₂ approaching to the Gra/Ca₂N. The red sphere in (a) denotes the O atom. In (b), d_0 is the optimal distance. (d) The adsorption energies, for H, O₂, and CO on Gra/Ca₂N, the free-standing graphene, Li/BN and the free-standing BN monolayer.

We next study the CO oxidation reaction on the basal plane of graphene in Gra/Ca₂N heterojunction. We firstly evaluate the adsorption of O₂. Significantly, O₂ molecule is chemisorbed exothermically on Gra/Ca₂N heterojunction. It should be noted that its adsorption ability towards O₂ is found to be nearly independent on the adsorption sites with the adsorption energies $\sim 0.3 \text{ eV}$ [see Fig. S1 in Supporting Information]. The most stable configuration is shown in Fig. 2(a), from which we can

see the strong chemical bonds between C-O bonds from (1.53 Å), and the O-O bond (1.46 Å) is significantly elongated, compared with the free O₂ molecule (1.23 Å). We have further studied the O₂ adsorption under the various interlayer distances between graphene and Ca₂N, corresponding to the different energy intervals between the SVHS and E_F [see Fig. 1(f)]. With increasing in the interlayer distance, the adsorption energy of O₂ is significantly reduced [Fig. 2(b)]. It is suggested that tuning the position of SVHS with respect to E_F by external means could be an efficient strategy to modulate the catalytic behavior of SVHS. Moreover, Bader charge analysis³⁵ shows that there are 0.83 e⁻ transferred from the heterojunction to the adsorbed O₂, from the charge density difference, which mainly occupy its anti-bonding orbital [see Fig. 2(a)]. The evolution of the electronic states as a function of the distance between O₂ and Gra/Ca₂N is shown in Fig. 2(c). Obviously, once the O₂ approaching to Gra/Ca₂N, the major spin-down component of O₂ 2 π^* orbitals are gradually shifted below E_F , while the SVHS states shifted up with respect to E_F . This clearly indicates that the SVHS serves as an electronic bath to contribute to O₂ adsorption through electron transfer.

To consolidate the decisive role of SVHS catalysis on the CO oxidation, we study of the adsorption of H atom, O₂, and CO molecules on systems inheriting SVHS, including the aforementioned Gra/Ca₂N and Li intercalated bilayer boron nitride (Li/BN) [see Fig. S2 in Supporting Information], in comparison with their counterparts without the presence of SVHS, i.e., free-standing graphene and the free-standing BN. The systems with SVHS exhibit much higher adsorption energies than their counterparts without SVHS. Indeed, Li/BN with a SVHS laying 0.15 eV below E_F exhibits a drastic increase in H and O₂ adsorption energies by amount of 3.0 eV, compared with the intrinsic BN. In parallel, the binding strengths of H and O₂ on Gra/Ca₂N are enhanced by \sim 1.2 and 2.1 eV in comparison with the free-standing

graphene. We note that CO adsorption appears insensitive to the SVHS, which might be attributed to its weak oxidation nature³⁶⁻³⁷. These therefore highlight the effectiveness of the SVHS enabled chemical activity.

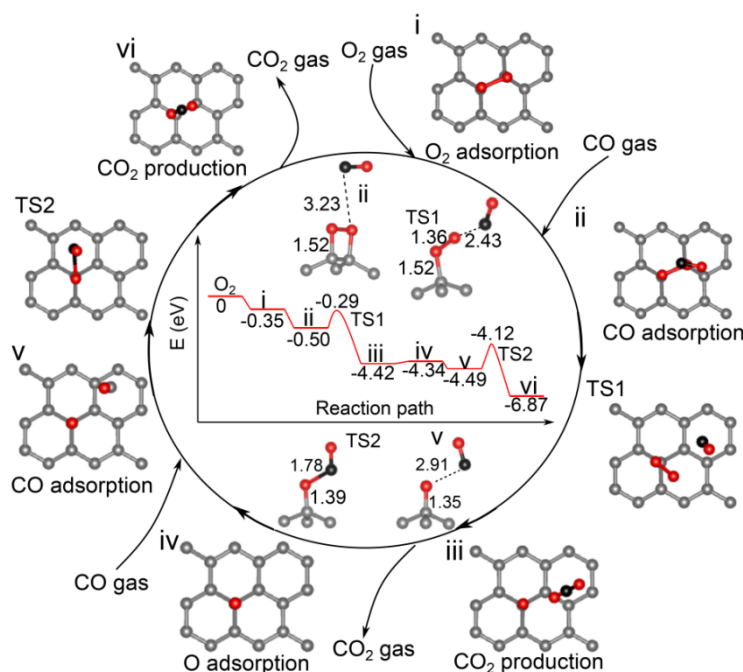


Figure 3: Catalytic cycle of CO oxidation on the Gra/Ca₂N. The transition states (TS) are marked, and the largest energy barrier is 0.37 eV for TS2. The insets in the cycle show the calculated energy profile and the configurations of the corresponding intermediates. The Ca₂N substrate is not shown for clarity.

It is well-established that there are two reaction mechanisms for CO oxidation by O₂, namely Langmuir-Hinshelwood (LH) and Eley-Rideal (ER) mechanisms³⁸⁻³⁹. The LH mechanism involves the co-adsorption of O₂ and CO molecules before reaction, while for the ER mechanism the free CO molecule directly reacts with the adsorbed O₂ molecule or O atom. Since the supported graphene only effectively bind O₂ molecule, the CO oxidation on the present heterojunction highly favors the ER mechanism. The reaction energy diagram along this pathway and the atomic configurations of the relevant intermediates are presented in Fig. 3. The incoming CO molecule directly attacks the pre-adsorbed O₂ species and is weakly adsorbed around O₂ molecule with

the energy release of 0.15 eV [see Fig. 3(i-ii)]. Upon overcoming an ultra-low energy barrier of 0.21 eV (TS1), the first CO₂ molecule can be readily produced [see Fig. 3(iii)]. After desorption of the outcome CO₂ molecule, the remaining O atom further reacts with the incoming CO molecule to produce the second CO₂ molecule [see Fig. 3 (iv-vi)] with an energy barrier of 0.37 eV (TS2), which is the rate-determining step for the whole CO oxidation reaction. Such low energy barriers allow the reaction to occur far below the room temperature, suggesting the important role of SVHS in the CO oxidation reaction.

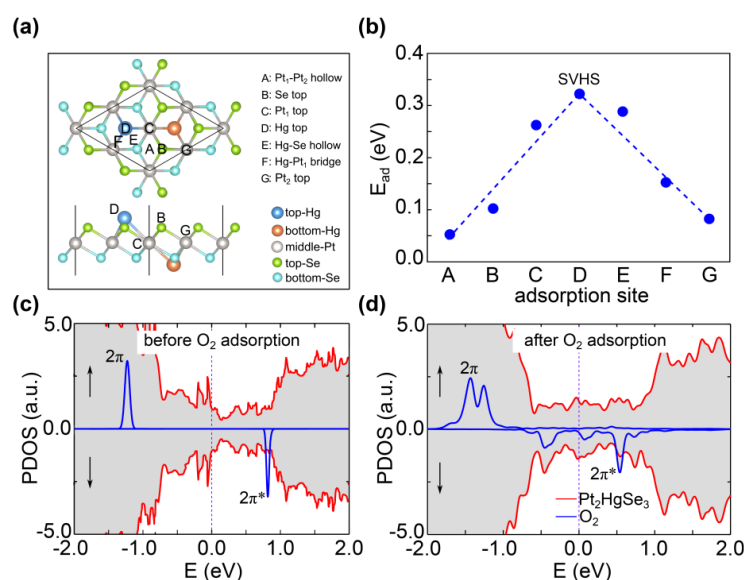


Figure 4: (a) Top and side views of the first layer of Pt₂HgSe₃ slab with the considered adsorption sites for O₂ from A to G. (b) The calculated adsorption energies of O₂ molecule on different adsorption sites of Pt₂HgSe₃ surface. (c) and (d) The PDOS of O₂ (blue line) and the first Pt₂HgSe₃ layer (red lines) before/after O₂ adsorption.

To further strengthen the viable role of SVHS in chemical reaction, we study the CO oxidation on Pt₂HgSe₃ (001) surface as another example. Fig. 4(a) shows the potential adsorption sites for O₂ and CO considered herein. It is found that only O₂ molecule is chemisorbed on the (001) surface by forming chemical bonds, similarly to the aforementioned heterojunction system. The O₂ adsorption energy is strongly site-

dependent (Fig. 4(b)), and peaks at the top of Hg atoms, as expected, where the charge density of SVHS mainly localizes (Fig. 1(d)). The calculated adsorption energy is 0.32 eV at this optimal adsorption position, which corresponds to 0.42 e^- transferring from the Pt₂HgSe₃ surface to fill the $2\pi^*$ anti-bonding orbital of O₂ molecule [see Figs. 4(c) and 4(d)]. The CO oxidation reaction following ER pathway is also favored on the Pt₂HgSe₃ (001) surface with a low energy barrier of ~ 0.6 eV [see Fig. S3 in Supporting Information]. Again, the SVHS in a distinct material system enables efficient CO oxidation.

In addition, we also studied the hydrogen evolution reaction (HER) on the Gra/Ca₂N heterojunction and Pt₂HgSe₃ (001) surface⁴⁰⁻⁴¹, for which the reaction activity is characterized by binding free energy of H (ΔG_H), that is high HER activity corresponds to vanishing ΔG_H (in absolute value), and vice versa⁴¹⁻⁴². The results presented in Fig. S4 show that the free-standing graphene is extremely inert towards HER with $\Delta G_H \sim 1.7$ eV⁴¹, while, as expected, the SVHS in the supported graphene can significantly enhance the hydrogen binding strength (to ~ 0.1 eV) and the HER activity. Similarly, the topological Pt₂HgSe₃ (001) surface is also highly favorable with ΔG_H being as low as 0.16 eV at the Hg site [see Fig. S4(b)]. We hence have justified the viable role of SVHS in catalytic reactions, irrespectively of CO oxidation and HER.

Apart from the Gra/Ca₂N and Pt₂HgSe₃ (001) surface, other material systems with SVHS have been explored, such as Li/BN¹⁸, alkali-metal intercalated graphene on SiC¹⁷, twisted graphene bilayer¹⁵⁻¹⁶, graphene/Y₂C electride heterojunction [see Fig. S5 in Supporting Information], Sn/p-type Si(111)¹² and Pb₃Bi/Ge(111)¹³. Given different orbital characteristics and its strong localization properties of SVHS, these systems are expected to possess distinct chemical activities toward different gas molecules (Fig. 2d), and be applied in different catalytic reactions. As an example, Li/BN with SVHS

exhibits an ultrahigh reactivity towards the extreme inert N_2 molecule, with an adsorption energy of ~ 1.6 eV [see Fig. S2 in Supporting Information]. Such a platform may be capable for efficient ammonia synthesis, being motivated by recently discovered efficient conversion of N_2 to NH_3 using BN nanotubes filled with transition metal nanowires⁴³. Additionally, we foresee that the catalytic performance of Gra/ Ca_2N system constructed using twisted bilayer graphene instead of single graphene can be drastically enhanced considering the tunability nature of the position of VHS and the associated denser electronic states of twisted bilayer graphene reported in the recent experiments⁴⁴⁻⁴⁶.

Finally, we compile the promising signatures of SVHS catalysis after having discussed its effectiveness on CO oxidation. The first one is the well-defined active sites uniformly distributed over the whole surface. Indeed, the charge density is highly localized around the catalytically active sites which are well-defined, as already shown in Figs. 1(c) and (d) for Gra/ Ca_2N and Pt_2HgSe_3 (001) surface, respectively. This feature therefore makes SVHS catalysis outperform most of prevailing catalytic schemes with strongly localized active sites, such as heteroatom doping and atomic vacancy, which are distributed randomly and hard to identify^{42, 47-48}. The other is the tunability nature of the catalytic activity with controlling the relative energy position of SVHS with respect to E_F . This can be inferred from the tunability of the O_2 binding strength and, simultaneously, the energy interval between SVHS and E_F , with the variation of interlayer distance in Gra/ Ca_2N , as shown in Figs. 1(f) and 2(b).

To conclude, we demonstrate the SVHS catalysis through systematically studying CO oxidation reaction on the Gra/ Ca_2N heterojunction and Pt_2HgSe_3 (001) surface. SVHS serving as an electron bath enables O_2 chemisorption and subsequently efficient CO oxidation, as justified by the low energy barriers of the rate-determining steps in

the range of 0.2 ~ 0.6 eV for both material systems. The SVHS catalysis exhibits intriguing features of well-defined active sites, associated with the electronic states of SVHS, and tunability nature with controlling the relative energy position of SVHS with respect to E_F . The present work enriches the Van Hove physics in material systems with reduced dimensions, and provides a new approach for the design of catalysts guided by the material electronic properties, beyond the d-band center theory.

Acknowledgement

We thank Prof. Zhenyu Zhang at University of Science and Technology of China for helpful discussion. This work was supported by National Natural Science Foundation of China (Nos. 11774078, 11704005, and 11804077), China Postdoctoral Science Foundation (No. 2020M672201).

References

1. Van Hove, L. The Occurrence of Singularities in the Elastic Frequency Distribution of a Crystal. *Phys. Rev.* **1953**, *89* (6), 1189-1193.
2. McChesney, J. L.; Bostwick, A.; Ohta, T.; Seyller, T.; Horn, K.; González, J.; Rotenberg, E. Extended van Hove Singularity and Superconducting Instability in Doped Graphene. *Phys. Rev. Lett.* **2010**, *104* (13), 136803.
3. Akashi, R. Archetypical "Push the Band Critical Point" Mechanism for Peaking of the Density of States in Three-dimensional Crystals: Theory and Case Study of Cubic H₃S. *Phys. Rev. B* **2020**, *101* (7), 075126.
4. Irkhin, V. Y.; Katanin, A. A.; Katsnelson, M. I. Robustness of the Van Hove Scenario for High-T_c Superconductors. *Phys. Rev. Lett.* **2002**, *89* (7), 076401.
5. Markiewicz, R. S. A Survey of the Van Hove Scenario for High-T_c

Superconductivity with Special Emphasis on Pseudogaps and Striped Phases. *J. Phys. Chem. Solids* **1997**, *58* (8), 1179-1310.

6. Fleck, M.; Oleś, A. M.; Hedin, L. Magnetic Phases near the Van Hove Singularity in s- and d-band Hubbard Models. *Phys. Rev. B* **1997**, *56* (6), 3159-3166.

7. Wang, W.-S.; Li, Z.-Z.; Xiang, Y.-Y.; Wang, Q.-H. Competing Electronic Orders on Kagome Lattices at Van Hove Filling. *Phys. Rev. B* **2013**, *87* (11), 115135.

8. Markiewicz, R. S. Phase Separation near the Mott Transition in $\text{La}_{2-x}\text{Sr}_x\text{CuO}_4$. *J. Phys. Condens. Matter* **1990**, *2* (3), 665-676.

9. Ludbrook, B. M.; Levy, G.; Nigge, P.; Zonno, M.; Schneider, M.; Dvorak, D. J.; Veenstra, C. N.; Zhdanovich, S.; Wong, D.; Dosanjh, P.; Straßer, C.; Stöhr, A.; Forti, S.; Ast, C. R.; Starke, U.; Damascelli, A. Evidence for Superconductivity in Li-decorated Monolayer Graphene. *Proc. Natl. Acad. Sci. U. S. A.* **2015**, *112* (38), 11795.

10. Rosenzweig, P.; Karakachian, H.; Link, S.; Küster, K.; Starke, U. Tuning the Doping Level of Graphene in the Vicinity of the Van Hove Singularity via Ytterbium Intercalation. *Phys. Rev. B* **2019**, *100* (3), 035445.

11. Link, S.; Forti, S.; Stöhr, A.; Küster, K.; Rösner, M.; Hirschmeier, D.; Chen, C.; Avila, J.; Asensio, M. C.; Zakharov, A. A.; Wehling, T. O.; Lichtenstein, A. I.; Katsnelson, M. I.; Starke, U. Introducing Strong Correlation Effects into Graphene by Gadolinium Intercalation. *Phys. Rev. B* **2019**, *100* (12), 121407.

12. Wu, X.; Ming, F.; Smith, T. S.; Liu, G.; Ye, F.; Wang, K.; Johnston, S.; Weiering, H. H. Superconductivity in a Hole-Doped Mott-Insulating Triangular Adatom Layer on a Silicon Surface. *Phys. Rev. Lett.* **2020**, *125* (11), 117001.

13. Qin, W.; Li, L.; Zhang, Z. Chiral Topological Superconductivity Arising from the Interplay of Geometric Phase and Electron Correlation. *Nat. Phys.* **2019**, *15* (8), 796-802.

14. Wang, F.; Zhang, Y.; Tian, C.; Girit, C.; Zettl, A.; Crommie, M.; Shen, Y. R. Gate-Variable Optical Transitions in Graphene. *Science* **2008**, *320* (5873), 206.
15. Li, G.; Luican, A.; Lopes dos Santos, J. M. B.; Castro Neto, A. H.; Reina, A.; Kong, J.; Andrei, E. Y. Observation of Van Hove Singularities in Twisted Graphene Layers. *Nat. Phys.* **2010**, *6* (2), 109-113.
16. Tan, Z.; Yin, J.; Chen, C.; Wang, H.; Lin, L.; Sun, L.; Wu, J.; Sun, X.; Yang, H.; Chen, Y.; Peng, H.; Liu, Z. Building Large-Domain Twisted Bilayer Graphene with Van Hove Singularity. *ACS Nano* **2016**, *10* (7), 6725-6730.
17. Profeta, G.; Calandra, M.; Mauri, F. Phonon-mediated Superconductivity in Graphene by Lithium Deposition. *Nat. Phys.* **2012**, *8* (2), 131-134.
18. Shimada, N. H.; Minamitani, E.; Watanabe, S. Theoretical Prediction of Phonon-Mediated Superconductivity with $T_C \approx 25$ K in Li-intercalated Hexagonal Boron Nitride Bilayer. *Appl. Phys. Express* **2017**, *10* (9), 093101.
19. Liao, L.; Wang, H.; Peng, H.; Yin, J.; Koh, A. L.; Chen, Y.; Xie, Q.; Peng, H.; Liu, Z. Van Hove Singularity Enhanced Photochemical Reactivity of Twisted Bilayer Graphene. *Nano Lett.* **2015**, *15* (8), 5585-5589.
20. Havener, R. W.; Liang, Y.; Brown, L.; Yang, L.; Park, J. Van Hove Singularities and Excitonic Effects in the Optical Conductivity of Twisted Bilayer Graphene. *Nano Lett.* **2014**, *14* (6), 3353-3357.
21. Kim, K.; Coh, S.; Tan, L. Z.; Regan, W.; Yuk, J. M.; Chatterjee, E.; Crommie, M. F.; Cohen, M. L.; Louie, S. G.; Zettl, A. Raman Spectroscopy Study of Rotated Double-Layer Graphene: Misorientation-Angle Dependence of Electronic Structure. *Phys. Rev. Lett.* **2012**, *108* (24), 246103.
22. Li, L.; Ren, S.; Qin, W.; Zhang, S.; Wan, X.; Jia, Y.; Cui, P.; Zhang, Z. Emergence of Van Hove Singularity and Topological States in $Pb_3Bi/Ge(111)$ Rashba Systems.

Phys. Rev. B **2020**, *102* (3), 035150.

23. González, J. Charge-density-wave Formation by Van Hove Nesting in the a-phase of Sn/Ge(111). *Phys. Rev. B* **2000**, *62* (11), 6928-6931.

24. Inoshita, T.; Tsukada, M.; Saito, S.; Hosono, H. Probing a Divergent Van Hove Singularity of Graphene with a Ca₂N Support: A Layered Electride as A Solid-State Dopant. *Phys. Rev. B* **2017**, *96* (24), 245303.

25. Kim, S.; Park, J.; Duong, D. L.; Cho, S.; Kim, S. W.; Yang, H. Proximity Engineering of the Van Der Waals Interaction in Multilayered Graphene. *ACS Appl. Mater. Interfaces* **2019**, *11* (45), 42528-42533.

26. Ghosh, B.; Mardanya, S.; Singh, B.; Zhou, X.; Wang, B.; Chang, T.-R.; Su, C.; Lin, H.; Agarwal, A.; Bansil, A. Saddle-point Van Hove Singularity and Dual Topological State in Pt₂HgSe₃. *Phys. Rev. B* **2019**, *100* (23), 235101.

27. Cucchi, I.; Marrazzo, A.; Cappelli, E.; Riccò, S.; Bruno, F. Y.; Lisi, S.; Hoesch, M.; Kim, T. K.; Cacho, C.; Besnard, C.; Giannini, E.; Marzari, N.; Gibertini, M.; Baumberger, F.; Tamai, A. Bulk and Surface Electronic Structure of the Dual-Topology Semimetal Pt₂HgSe₃. *Phys. Rev. Lett.* **2020**, *124* (10), 106402.

28. Chen, H.; Zhu, W.; Xiao, D.; Zhang, Z. CO Oxidation Facilitated by Robust Surface States on Au-Covered Topological Insulators. *Phys. Rev. Lett.* **2011**, *107* (5), 056804.

29. Li, J.; Ma, H.; Xie, Q.; Feng, S.; Ullah, S.; Li, R.; Dong, J.; Li, D.; Li, Y.; Chen, X.-Q. Topological Quantum Catalyst: Dirac Nodal Line States and a Potential Electrocatalyst of Hydrogen Evolution in the TiSi Family. *Sci. China Mater.* **2018**, *61* (1), 23-29.

30. Kresse, G.; Hafner, J. Ab Initio Molecular Dynamics for Open-shell Transition Metals. *Phys. Rev. B* **1993**, *48* (17), 13115-13118.

31. Kresse, G.; Furthmüller, J. Efficiency of Ab-initio Total Energy Calculations for Metals and Semiconductors Using a Plane-wave Basis Set. *Comput. Mater. Sci.* **1996**, *6* (1), 15-50.
32. Blöchl, P. E. Projector Augmented-Wave Method. *Phys. Rev. B* **1994**, *50* (24), 17953-17979.
33. Henkelman, G.; Uberuaga, B. P.; Jónsson, H. A Climbing Image Nudged Elastic Band Method for Finding Saddle Points and Minimum Energy Paths. *J. Chem. Phys.* **2000**, *113* (22), 9901-9904.
34. Castro Neto, A. H.; Guinea, F.; Peres, N. M. R.; Novoselov, K. S.; Geim, A. K. The electronic properties of graphene. *Reviews of Modern Physics* **2009**, *81* (1), 109-162.
35. Henkelman, G.; Arnaldsson, A.; Jónsson, H. A Fast and Robust Algorithm for Bader Decomposition of Charge Density. *Comp. Mater. Sci.* **2006**, *36* (3), 354-360.
36. Guo, N.; Xi, Y.; Liu, S.; Zhang, C. Greatly Enhancing Catalytic Activity of Graphene by Doping the Underlying Metal Substrate. *Scientific Reports* **2015**, *5* (1), 12058.
37. Guo, N.; Yam, K. M.; Zhang, C. Substrate engineering of graphene reactivity: towards high-performance graphene-based catalysts. *npj 2D Materials and Applications* **2018**, *2* (1), 1.
38. Mizuno, N.; Misono, M. Heterogeneous Catalysis. *Chem. Rev.* **1998**, *98* (1), 199-218.
39. Freund, H.-J.; Meijer, G.; Scheffler, M.; Schlögl, R.; Wolf, M. CO Oxidation as a Prototypical Reaction for Heterogeneous Processes. *Angew. Chem. Int. Ed.* **2011**, *50* (43), 10064-10094.
40. Voiry, D.; Salehi, M.; Silva, R.; Fujita, T.; Chen, M.; Asefa, T.; Shenoy, V. B.; Eda, G.; Chhowalla, M. Conducting MoS₂ Nanosheets as Catalysts for Hydrogen Evolution

Reaction. *Nano Lett.* **2013**, *13* (12), 6222-6227.

41. Jiao, Y.; Zheng, Y.; Davey, K.; Qiao, S.-Z. Activity Origin and Catalyst Design Principles for Electrocatalytic Hydrogen Evolution on Heteroatom-doped Graphene.

Nat. Energy **2016**, *1* (10), 16130.

42. Li, H.; Tsai, C.; Koh, A. L.; Cai, L.; Contryman, A. W.; Fragapane, A. H.; Zhao, J.; Han, H. S.; Manoharan, H. C.; Abild-Pedersen, F.; Nørskov, J. K.; Zheng, X. Activating and optimizing MoS₂ basal planes for hydrogen evolution through the formation of strained sulphur vacancies. *Nat. Mater.* **2016**, *15* (1), 48-53.

43. Zhou, S.; Yang, X.; Xu, X.; Dou, S. X.; Du, Y.; Zhao, J. Boron Nitride Nanotubes for Ammonia Synthesis: Activation by Filling Transition Metals. *J. Amer. Chem. Soc.* **2020**, *142* (1), 308-317.

44. Cao, Y.; Fatemi, V.; Fang, S.; Watanabe, K.; Taniguchi, T.; Kaxiras, E.; Jarillo-Herrero, P. Unconventional superconductivity in magic-angle graphene superlattices. *Nature* **2018**, *556* (7699), 43-50.

45. Choi, Y.; Kemmer, J.; Peng, Y.; Thomson, A.; Arora, H.; Polski, R.; Zhang, Y.; Ren, H.; Alicea, J.; Refael, G.; von Oppen, F.; Watanabe, K.; Taniguchi, T.; Nadj-Perge, S. Electronic correlations in twisted bilayer graphene near the magic angle. *Nature Physics* **2019**, *15* (11), 1174-1180.

46. Lisi, S.; Lu, X.; Benschop, T.; de Jong, T. A.; Stepanov, P.; Duran, J. R.; Margot, F.; Cucchi, I.; Cappelli, E.; Hunter, A.; Tamai, A.; Kandyba, V.; Giampietri, A.; Barinov, A.; Jobst, J.; Stalman, V.; Leeuwenhoek, M.; Watanabe, K.; Taniguchi, T.; Rademaker, L.; van der Molen, S. J.; Allan, M. P.; Efetov, D. K.; Baumberger, F. Observation of flat bands in twisted bilayer graphene. *Nature Physics* **2021**, *17* (2), 189-193.

47. McFarland, E. W.; Metiu, H. Catalysis by Doped Oxides. *Chem. Rev.* **2013**, *113* (6), 4391-4427.

48. Wang, X.; Sun, G.; Routh, P.; Kim, D.-H.; Huang, W.; Chen, P. Heteroatom-doped Graphene Materials: Syntheses, Properties and Applications. *Chem. Soc. Rev.* **2014**, *43* (20), 7067-7098.